Natural convection and entropy generation inside porous square cavity with undulated vertical walls under four heating scenarios

Mouna Maache[a], *Chihab* Eddine Brahmi[b], *Nourredine* Belghar[c], *Mahmoud* Kalfali[d]

Faculty of Science and Technology, Department of Mechanical Engineering, Abbes Laghrour University, Khenchela, Algeria

[a] e-mail: mouna.maache@univ-khenchela.dz, **corresponding author**,
ORCID iD: https://orcid.org/0000-0002-6466-1719

[b] e-mail: brahmi.chihabeddine@univ-khenchela.dz,
ORCID iD: https://orcid.org/0009-0003-3578-8440

[c] e-mail: belghar.nourredine@univ-khenchela.dz,
ORCID iD: https://orcid.org/0000-0002-7772-5101

[d] e-mail: kalfali.mahmoud@univ-khenchela.dz,
ORCID iD: https://orcid.org/0009-0002-6183-7800

https://doi.org/10.5937/vojtehg74-58738

FIELD: mechanics, mechanical engineering
ARTICLE TYPE: original scientific paper

Abstract:

Introduction/purpose: This work studies natural convection within a porous cavity with undulated vertical walls focusing on investigating the effects of various heating scenarios. The model consists of a square cavity with sinusoidal undulations on its vertical walls. The cavity is characterized by a square cross-section, and the undulations are described by a sinusoidal wave function with a specific amplitude and wavelength. The left vertical wall of the cavity is maintained at a constant cold temperature, while the bottom wall is subjected to various heating profiles, including linear heating, constant heating, parabolic heating, and sinusoidal heating. The choice of these different heating scenarios is intended to explore how the heat transfer behavior changes under each condition. The top and right walls are assumed to be adiabatic.

Methods: The effects of heating methods and Darcy number on fluid flow and heat transfer in the cavity under a high Rayleigh number are numerically analyzed.

Results: Results show that all heating profiles create distinct thermal gradients, influencing the vortex strength and flow complexity. The study also investigates the irreversibilities within the system, focusing on entropy generation due to both heat transfer and fluid friction, to evaluate the thermodynamic efficiency of the cavity.

Conclusion: The study aims to provide a comprehensive understanding of how heating conditions, permeability variations and high Rayleigh number convection affect the thermal and fluid dynamics in porous cavities, with implications for improving the performance of thermal management systems in practical engineering applications.

Key words: cavity, porous medium, free convection, entropy generation, porosity, permeability.

Introduction

Heat transfer in porous media is a fundamental physical phenomenon that has developed over time. Whether in geothermal energy systems (Böttcher et al, 2016), agricultural soil management (Abed Gatea Al-Shammary et al, 2020), building insulation (Kumar et al, 2020; Pichler et al, 2012) or underground thermal storage (Bloemendal et al, 2014), heat movement plays a critical role in determining energy efficiency, environmental sustainability, and overall system performance. Heat transfer typically occurs through a variety of mechanisms. In complex systems such as porous media, these mechanisms often interact in complex ways, posing significant challenges for accurate modeling and prediction.

Heat transfer and fluid flow in porous media are governed by several factors, such as local thermal equilibrium or non-equilibrium (Gao et al, 2013), time, porosity, tortuosity and permeability, and other properties (Massoud Kaviany, 2011). The complexity is further enhanced by the interplay of thermal conduction, convection, and sometimes radiation within the porous matrix.

Recent advances in heat transfer research increasingly focus on understanding entropy generation mechanisms in porous enclosures under diverse thermal and geometric configurations. Basak et al. (2011), Kaluri & Basak (2011), Brahmi et al. (2024), and Dutta et al. (2021) investigate natural convection and entropy generation in various porous enclosures under different thermal boundary conditions, geometries, and heating methods. Key findings highlight that entropy generation is mainly influenced by heat transfer irreversibility at low Darcy numbers, while fluid friction becomes dominant at higher Darcy and Rayleigh numbers. Factors such as cavity shape, wall undulations, and non-uniform heating with phase shifts significantly affect heat transfer efficiency and entropy production, with optimal configurations minimizing irreversibility.

Extending these insights, Tasmin et al. (2021) incorporate nanofluids and non-Newtonian effects in a wavy porous cavity, demonstrating that lower power-law indices and higher nanoparticle concentrations enhance

heat transfer, with heat transfer irreversibility remaining dominant. Similarly, Al-Waaly et al. (2024) show that optimizing the heated segment length in triangular porous cavities improves thermal performance and reduces entropy generation. In contrast, Rashad et al. (2024) examine magneto-convective effects in nanofluid-filled inclined porous cavities, revealing that magnetic field strength and nanoparticle concentration can diminish heat transfer, highlighting the importance of strategic heat source and sink placement to control entropy generation.

However, despite these advances, limited attention has been given to the combined influence of high Rayleigh number convection, wall undulations, and different heating modes in porous cavities. Most existing studies have considered either simple geometries or uniform heating conditions, while the interplay between sinusoidal boundary geometries and non-uniform heating scenarios under varying permeability remains insufficiently explored.

This study numerically investigates the thermal and fluid flow behavior in a porous square cavity with sinusoidal vertical walls, each having four undulations. The cavity is cooled by a constant cold temperature Tc on the left vertical wall, while the bottom wall is subjected to varying heating scenarios, including linear, constant, parabolic, and sinusoidal heating, while the other walls are maintained insulated. This analysis is conducted under a high Rayleigh number condition ($Ra = 10^6$), which promotes natural convection, and focuses on the impact of different permeability levels, characterized by three values of Darcy numbers ($Da = 10^{-5}$, 10^{-3} and 10^{-1}). The study aims to understand how the combination of porous medium properties and heating conditions influences heat transfer within the cavity at high Rayleigh number. Specifically, the study seeks to explore the effects of different heating types on temperature distribution and flow patterns, examine the role of permeability variations in shaping convective heat transfer, and analyses the resulting flow and thermal fields using isotherms and streamlines. Furthermore, the performance of the system is assessed by calculating both local and average Nusselt numbers to quantify the convective heat transfer efficiency. The study also investigates the irreversibilities within the system, focusing on entropy generation due to both heat transfer and fluid friction, to evaluate the thermodynamic efficiency of the cavity. Ultimately, the study aims to provide a comprehensive understanding of how heating conditions, permeability variations, and high Rayleigh number convection affect the thermal and fluid dynamics in porous cavities, with implications for improving the performance of thermal management systems in practical engineering applications.

Problem description

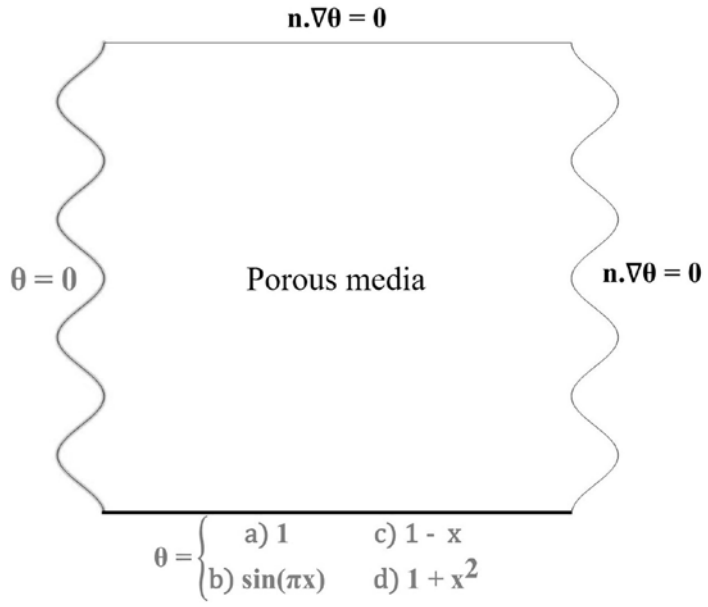

Figure 1 – Schematic of the undulated square porous cavity with four undulations on the vertical walls

Simplifying assumptions

- Fluid is a Newtonian, incompressible, steady, laminar, and two-dimensional.
- All properties are constant, except density, which varies based on the Boussinesq approximation.
- The extended Darcy–Brinkman–Forchheimer model governs the entire domain for momentum transfer.
- Local thermal equilibrium (LTE) is assumed between fluid and solid phases.
- Viscous dissipation is neglected.
- The entire domain of the physical model consists of a porous medium with irregular vertical walls.

Equations in dimensionless form

Based on the simplifying assumptions, the governing equations (Chen et al. 2008) for flow and heat transfer, applicable to the geometries illustrated in Figure 1, are expressed below using a Cartesian coordinate system:

Continuity equation

This equation ensures mass conservation in the fluid:

$$\frac{\partial U}{\partial X} + \frac{\partial V}{\partial Y} = 0 \tag{1}$$

Momentum equations

The Extended Darcy–Brinkman–Forchheimer model is used to account for momentum transfer in the porous media:

- It includes Darcy drag to account for flow resistance due to the porous matrix.
- Incorporates Brinkman viscous effects, which describe velocity gradients in the porous medium.
- Accounts for Forchheimer inertial resistance to represent non-linear drag effects at higher velocities.

Momentum formulation along the x-axis

$$\frac{\partial}{\partial X}\left(\frac{UU}{\varepsilon}\right) + \frac{\partial}{\partial Y}\left(\frac{VU}{\varepsilon}\right) = -\frac{\partial P}{\partial X} + Pr\left(\frac{\partial^2 U}{\partial X^2} + \frac{\partial^2 U}{\partial Y^2}\right) - U\,\varepsilon\,\frac{Pr}{Da} - \frac{1.75}{\sqrt{150}}\,\frac{U\sqrt{(U^2+V^2)}}{\sqrt{Da\cdot\varepsilon}} \tag{2}$$

Momentum formulation along the y-axis

$$\frac{\partial}{\partial X}\left(\frac{UV}{\varepsilon}\right) + \frac{\partial}{\partial Y}\left(\frac{VV}{\varepsilon}\right) = -\frac{\partial P}{\partial Y} + Pr\left(\frac{\partial^2 V}{\partial X^2} + \frac{\partial^2 V}{\partial Y^2}\right) -$$

$$V\,\varepsilon\,\frac{Pr}{Da} + Ra\,Pr\;\varepsilon\;\theta - \frac{1.75}{\sqrt{150}}\,\frac{U\sqrt{(U^2+V^2)}}{\sqrt{Da\cdot\varepsilon}} \tag{3}$$

Energy equation

In the porous region:

$$U\,\frac{\partial \theta}{\partial X} + V\,\frac{\partial \theta}{\partial Y} = R_k\left(\frac{\partial^2 \theta}{\partial X^2} + \frac{\partial^2 \theta}{\partial Y^2}\right) \tag{4}$$

In the fluid region:

$$U\,\frac{\partial \theta}{\partial X} + V\,\frac{\partial \theta}{\partial Y} = \frac{\partial^2 \theta}{\partial X^2} + \frac{\partial^2 \theta}{\partial Y^2} \tag{5}$$

Stream function

The Stream function, denoted by the symbol ψ, offers a visual representation of fluid motion within the cavities. For two-dimensional flows, it is defined as below:

$$\frac{\partial^2 \psi}{\partial X^2} + \frac{\partial^2 \psi}{\partial Y^2} = \frac{\partial U}{\partial Y} - \frac{\partial V}{\partial X} \tag{6}$$

Boundary conditions

Bottom boundary (various heating conditions):

U = V = 0. $\theta = \begin{pmatrix} 1 \\ 1-x \\ 1+x^2 \\ sin(\pi\, x) \end{pmatrix}$

Top boundary (adiabatic):

U = V = 0. $\partial\theta/\partial n = 0$

Side walls:

U = V = 0.

At the left wall: $\theta = 0$ At the right wall: $\partial\theta/\partial n = 0$

Nusselt number

The local Nusselt number is calculated from the temperature gradient to assess the heat transfer along the cavity boundaries. It is calculated as follows:

$$Nu_L = -\frac{\partial\theta}{\partial n} \tag{7}$$

where $\frac{\partial}{\partial \mathrm{n}}$ represents the dimensionless derivative taken in the direction of the outward normal to the surface under consideration.

The average Nusselt number is the mean of the local Nusselt number along a wall and it is defined by Bhardwaj et al. (2015) as:

$$Nu_{avg} = \frac{1}{L}\int_0^L Nu_L\, dl \tag{8}$$

Heat transfer irreversibility

This type of irreversibility occurs due to non-uniform temperature distributions, leading to entropy generation. It is symbolized as S_{hti}. This irreversibility is formulated by Bejan, A. (1979) as:

$$S_{hti} = \left[\left(\frac{\partial\theta}{\partial X}\right)^2 + \left(\frac{\partial\theta}{\partial Y}\right)^2\right] \tag{9}$$

Fluid friction irreversibility

This irreversibility arises from viscous effects and velocity gradients within the fluid, contributing to entropy generation. It is denoted as S_{ffi}. The formulation for this irreversibility is:

$$S_{ffi} = \xi\left[(U^2+V^2) + Da\left\{2\left(\left(\frac{\partial U}{\partial X}\right)^2 + \left(\frac{\partial V}{\partial Y}\right)^2\right) + \left(\frac{\partial U}{\partial Y} + \frac{\partial V}{\partial X}\right)^2\right\}\right] \tag{10}$$

Here, ξ is the irreversibility distribution ratio, defined as:

$$\xi = \frac{\mu T_0}{K}\left(\frac{\alpha}{\sqrt{K}\Delta T}\right)^2 \quad (11)$$

The entropy generation rate resulting from the combined contributions of these sources is denoted by S. This is expressed by the equation:

$$S = S_{hti} + S_{ffi} \quad (12)$$

S_T is the total entropy generation within these porous cavities can be derived as:

$$S_T = S_{hti_{total}} + S_{ffi_{total}} \quad (13)$$

where:

$$S_{hti_{total}} = \int_{\Omega} S_{hti}\, d\Omega \quad (14)$$

To assess the irreversibility distribution, the Bejan number (Be) represents the ratio of heat transfer irreversibility to the sum of the two contributors of entropy generation. Through analyzing the distribution of local entropy generation, the Bejan number is derived as follows:

$$Be = \frac{S_{hti}}{S_{hti}+S_{ffi}} \quad (15)$$

Then, average Bejan number is given by:

$$Be_{avg} = \frac{S_{hti_{total}}}{S_{hti_{total}}+S_{ffi_{total}}} \quad (16)$$

The value of Be_{avg} ranges between [0, 1]. When $Be_{avg} < 0.5$, heat transfer irreversibility is the dominant contributor to entropy generation. Conversely, when $Be_{avg} > 0.5$, fluid friction irreversibility becomes the primary source of entropy generation.

The numerical simulations software

The numerical simulations were carried out using the finite element method (FEM) implemented through the COMSOL Multiphysics® software. FEM is a well-established technique for solving partial differential equations over complex geometries, making it particularly suitable for modelling heat transfer in porous media. This method divides the computational domain into smaller subdomains (elements), ensuring accurate spatial resolution and efficient handling of irregular boundaries.

COMSOL Multiphysics® was selected for its robust FEM-based solver and its ability to couple various physics phenomena. Its user friendly interface and built-in modules allow for rapid prototyping and reliable

simulation of coupled thermal and flow processes in porous cavities. These features make COMSOL Multiphysics® a versatile tool for this study.

Findings and interpretation

Mesh consistency analysis

A mesh independence analysis was conducted to ensure the reliability and accuracy of the numerical results. Simulations were performed using varying mesh densities, and the results were compared to evaluate convergence. For this study, the computational domain employs a non-orthogonal grid tailored to accommodate the geometric irregularities of the enclosure's undulated side walls.

The convergence test focused on assessing natural convection within a 2D porous cavity with sinusoidal heating applied to the bottom wall, a cold left wall, and adiabatic (insulated) conditions on the remaining walls. The analysis was performed using specific parameters: porosity $(\varepsilon = 0.9)$, $(Pr = 0.71)$, $(Ra = 10^6)$ and $(Da = 10^{-2})$.

The mean Nusselt number along the heated bottom wall served as the evaluation metric for convergence. A range of mesh configurations, with discretization levels of 80, 120, 160, 200, 240, 280, 300, and 320 elements per side was tested to ensure consistency and precision in the numerical results.

The analysis demonstrated, as shown in Table 1, that a mesh consisting of approximately 90000 (300×300) elements yields a converged solution, ensuring both accuracy and computational efficiency.

Table 1 – Comparison of the Nu_{avg} along heated bottom boundary for various grid sizes

Mesh	80×80	120×120	160×160	200×200	240×240	280×280	300×300	320×320
Nu_{avg}	8.816	9.088	9.264	9.399	9.478	9.601	9.642	9.648

Validation

To ensure the accuracy of the numerical results, a validation study was performed by comparing the findings with benchmark data from a two-dimensional porous triangular cavity. The cavity featured undulated vertical left walls, which were cooled, a sinusoidally heated bottom boundary, and adiabatic inclined side walls. The validation was conducted using a structured grid with 10 000 elements and through a parametric analysis under the conditions of Darcy number $(Da = 10^{-2})$, Prandtl number $(Pr = 0.71)$, and varying Rayleigh numbers. The local Nusselt

number distribution along the heated bottom boundary was compared with the results reported by Bhardwaj et al. (2015).

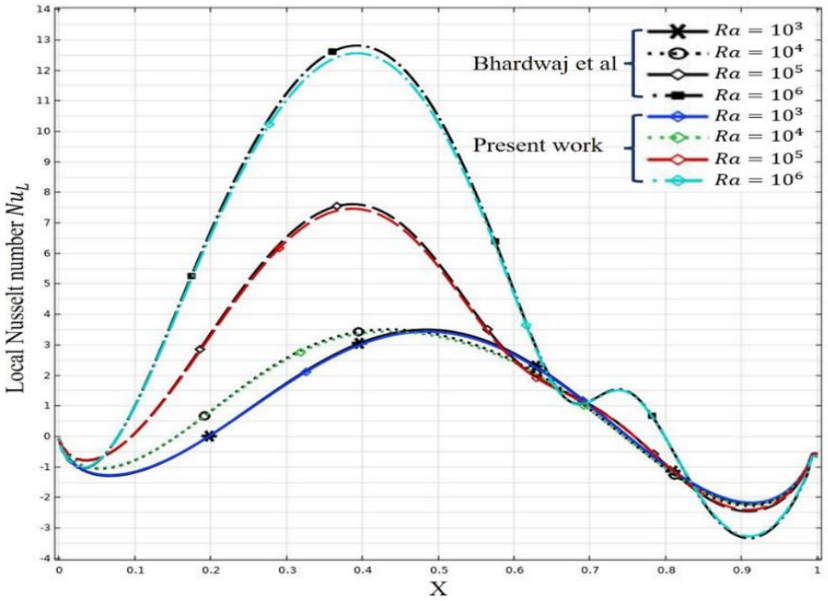

Figure 2 – Comparison between the current numerical simulation and those of Bhardwaj et al. (2015)

Isotherms and streamlines

The thermal and flow behavior within the side-wall undulated square cavity is significantly influenced by the heating conditions applied at the bottom wall. By analyzing the isotherms (Figure 3) and streamlines (Figure 4) for different permeability levels, characterized by Darcy numbers (Da = 10^{-5}, 10^{-3}, 10^{-1}), we can identify key trends in heat transfer and fluid motion across the four heating scenarios: constant heating, linear heating, parabolic heating, and sinusoidal heating.

Under constant heating ($\boldsymbol{\theta}$ = 1), where the bottom wall is maintained at a uniform hot temperature, the isotherms radiate outward from the lower-left corner at low permeability (Da = 10^{-5}). This pattern results from the high thermal gradient at the intersection of the hot and cold boundaries, leading to an unbounded heat flux at this singular point. As permeability increases, heat transfer transitions from conduction-dominated behavior to convective heat transfer, causing the isotherms to become more compact near the thermal boundaries.

The corresponding streamlines illustrate weak vortices at low permeability, indicating a suppression of convective motion due to the high resistance of the porous medium. However, as the permeability increases (Da = 10^{-1}), buoyancy-driven flow becomes more pronounced, strengthening the counterclockwise circulation within the cavity. This highlights the shift from conduction-dominated heat transfer at low permeability to convection-dominated transport at higher permeability.

In the case of linear heating (θ = 1 - x), where the temperature decreases along the bottom wall from left to right, the isotherms reveal a concentrated high-temperature region at the left side of the cavity. This localized heating effect drives fluid motion, creating two circulation cells: a smaller clockwise rotating vortex in the right region and a larger counterclockwise vortex in the left region.

At low permeability (Da = 10^{-5}), the streamlines indicate minimal fluid motion due to high flow resistance. However, as the permeability increases (Da = 10^{-1}), the buoyancy force strengthens, leading to a more dynamic circulation pattern. The intensity of the vortices rises from 17 at (Da = 10^{-3}) to nearly 49.94 at (Da = 10^{-1}), demonstrating that convective transport becomes increasingly dominant with higher permeability.

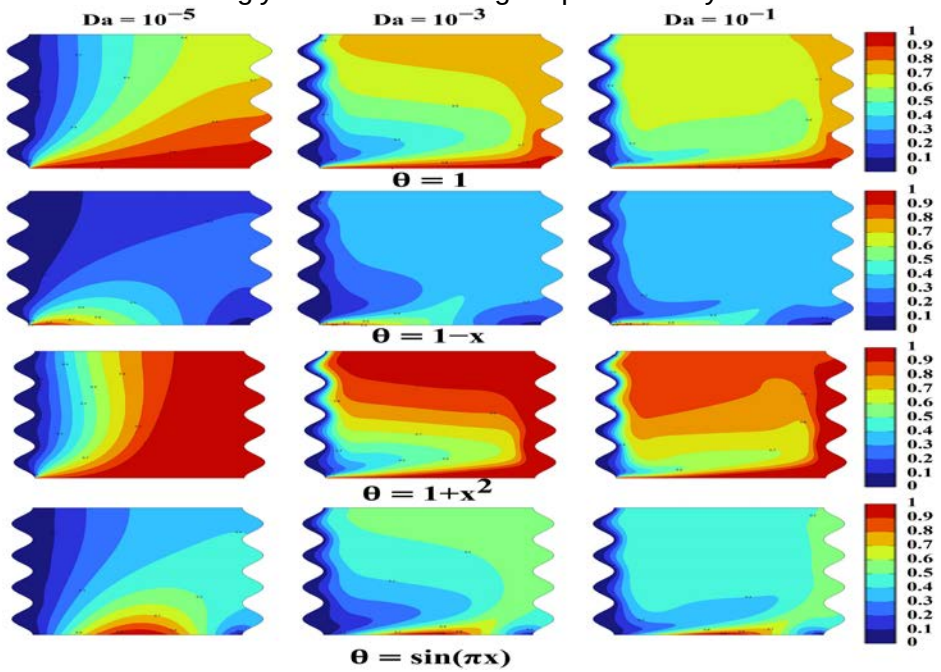

Figure 3 – Isothermal distributions under different heating conditions within the undulated square cavity filled by porous medium at Ra = 10^6

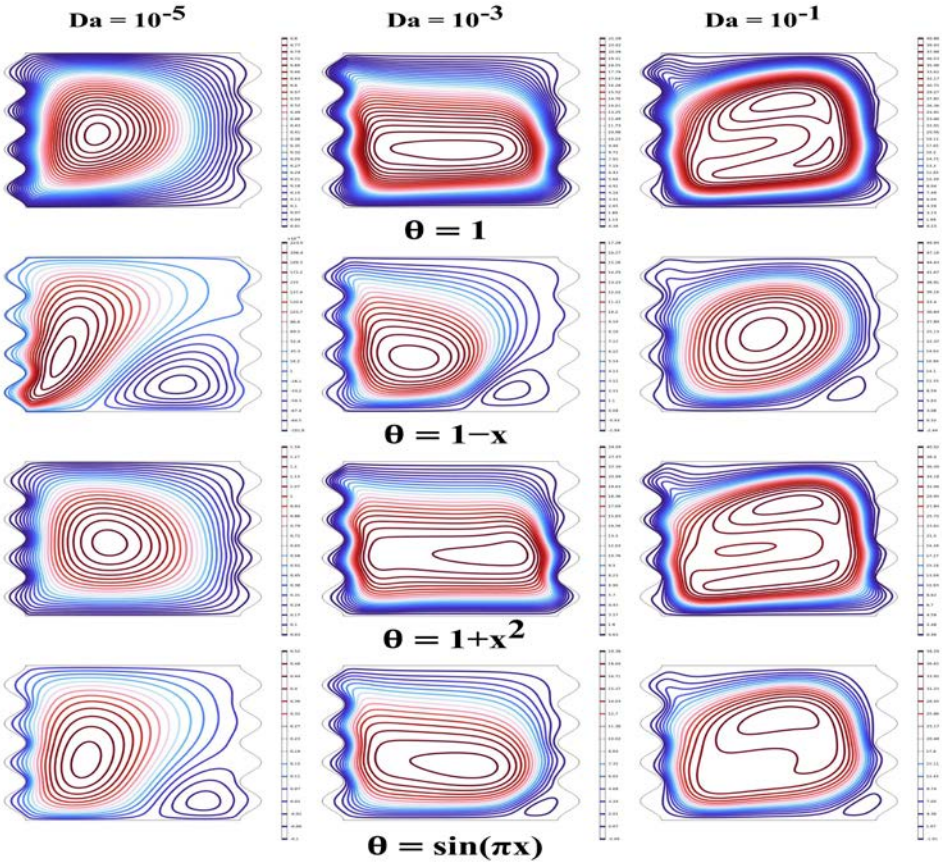

Figure 4 – Streamlines distributions under different heating conditions within the undulated square cavity filled by porous medium at Ra = 10^6

When a parabolic heating profile ($\theta = 1 + x^2$) is applied, the temperature gradient is steeper on the right side of the cavity, where heat accumulation is more pronounced. At low permeability (Da = 10^{-5}), limited fluid mobility results in localized thermal gradients, with conduction being the primary mode of heat transfer. As permeability increases (Da = 10^{-3}), stronger convective effects emerge, facilitating a counterclockwise circulation that redistributes thermal energy more efficiently.

At maximum permeability (Da = 10^{-1}), buoyancy forces are significantly enhanced, leading to a well-defined counterclockwise flow that ensures more uniform temperature distribution within the cavity. Compared to the other heating conditions, the parabolic heating case demonstrates a more localized thermal gradient, particularly in the right region, which governs the convective flow structure.

Under sinusoidal heating ($\boldsymbol{\theta}$ = Sin(πx)), where the bottom wall is subjected to a periodic temperature profile, the isotherms exhibit a distribution similar to that observed in the linear heating case. However, the key difference lies in the heat concentration, which is centered around the middle of the bottom wall rather than the left-hand side. This periodic heating results in alternating high and low-temperature zones, influencing the buoyancy-driven flow patterns.

The streamlines for sinusoidal and linear heating both display two counter-rotating vortices, one clockwise and one counterclockwise, driven by buoyancy forces. However, due to the periodic heating input, the sinusoidal case produces a more complex and oscillatory flow structure. Unlike linear heating, where the temperature gradient remains consistent along the heated surface, sinusoidal heating introduces fluctuations that create more intricate temperature zones and localized variations in fluid motion.

Nusselt number

Figure 5 presents the distributions of the local Nusselt number (Nu_L) for four heating scenarios, illustrating variations along (a) the hot bottom wall and (b) the cold left wall of the cavity for different Darcy numbers (Da = 10^{-5}, 10^{-3}, and 10^{-1}).

In subplots (a), Nu_L along the bottom wall generally decreases with increasing horizontal position (x) for all cases except when the heating profile follows (θ=sin(πx)).

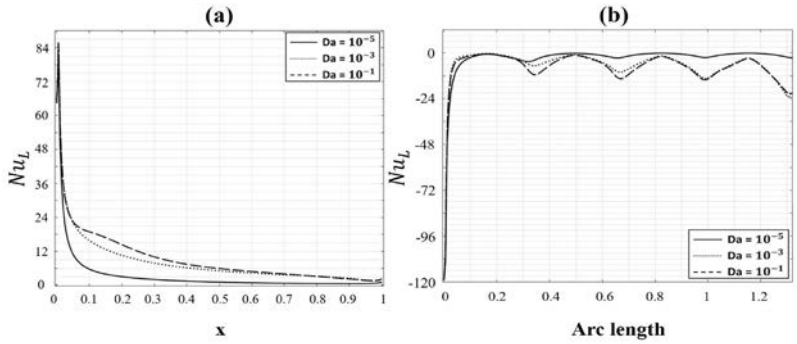

Case 1: $\theta = 1$

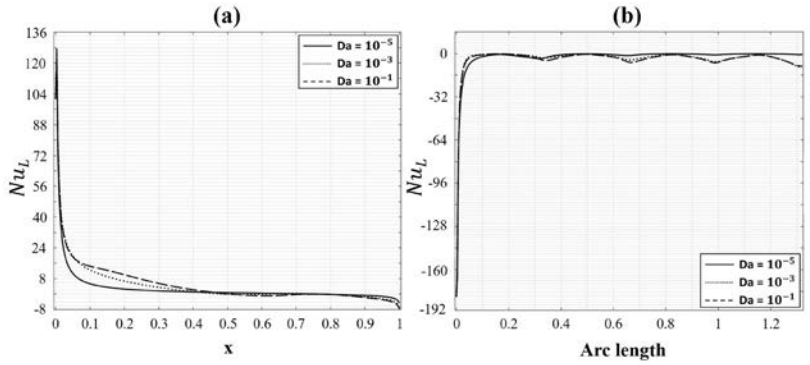

Case 2: $\theta = 1 - X$

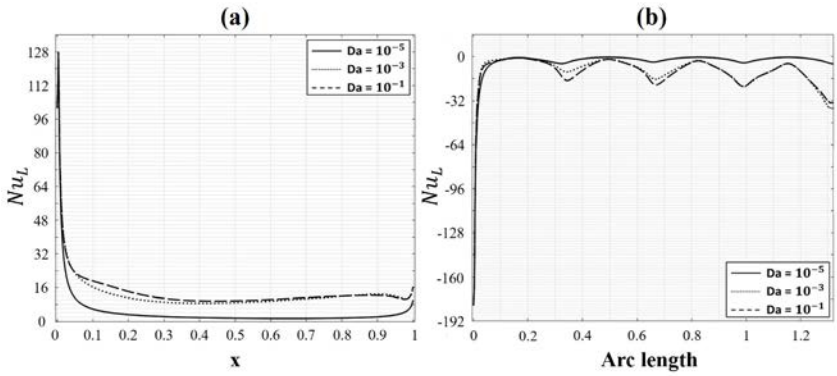

Case 3: $\theta = 1 + X^2$

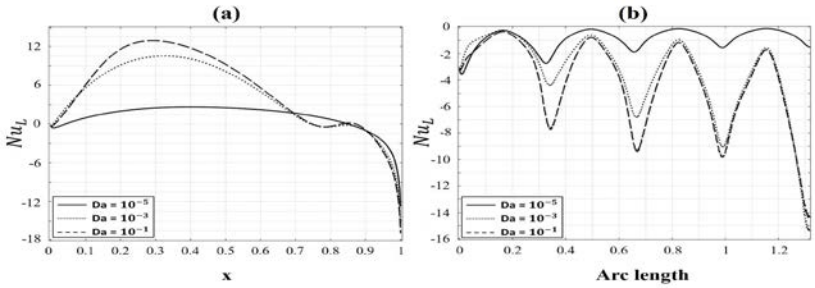

Case 4: $\theta = \sin(\pi X)$

Figure 5 – Nu_L distributions under different heating conditions along the bottom (a) and left (b) walls at Ra = 10^6

In this case, Nu_L initially increases on the left side before decreasing toward the right. This behavior directly corresponds to the oscillatory heating profile, where heat flux peaks coincide with the sinusoidal temperature maxima, producing alternating zones of enhanced and reduced heat transfer. Subplot (b) shows the Nu_L distribution along the cold left wall, where an oscillatory pattern is observed across all heating scenarios and Darcy numbers. Physically, these oscillations arise from the undulated geometry of the cold wall, which alternately accelerates and decelerates heat transfer by modifying local boundary layer thickness. As Da increases, the amplitude of these oscillations grows due to the influence of the undulated cold wall. A sharp decline in Nu_L near the bottom edges is likely caused by overlapping heating and cooling effects. Additionally, a higher Da reduces the sharp drop in Nu_L by enhancing buoyancy-driven convection, which facilitates heat transfer. The negative Nu_L values indicate a reversal in heat transfer direction, signifying that heat flows from the fluid to the cold wall rather than the reverse. This effect is driven by the cooling impact of the wall and buoyancy forces. Among the tested heating scenarios, the sinusoidal heating case results in the least pronounced Nu_L distribution along the cold wall, since the periodic input smooths out extreme gradients, distributing heat more evenly compared to localized heating cases.

Average Nusselt number

At a high Rayleigh number of 10^6, the two graphs present distinct yet complementary thermal behaviors, (a) along the heated bottom wall and (b) on the undulated cold vertical wall of the porous cavity under varying permeability and heating scenarios. Along the bottom boundary, the average Nusselt number is positive, indicating net heat release into the fluid, and its magnitude increases with permeability as higher Darcy numbers reduce flow resistance, intensify buoyancy-driven circulation, and thin the thermal boundary layer. Conversely, along the cold vertical wall, the Nusselt number is negative, reflecting heat absorption from the fluid, with its absolute value likewise growing with permeability due to stronger impingement of hot plumes. In both cases, the heating mode significantly influences convective performance: parabolic heating produces the strongest enhancement, followed by constant heating, while linear and sinusoidal distributions yield comparatively weaker transfer rates. The wall undulation further augments heat exchange by enlarging the effective surface area and generating local recirculation zones, particularly under high permeability. Overall, the comparison reveals that both boundaries

exhibit analogous trends governed by the same convective mechanisms, with opposite heat flux directions, and that parabolic heating consistently maximizes global heat transfer efficiency. These observations are in good agreement with the streamline and isothermal contour distributions, which clearly demonstrate intensified circulation cells and sharper thermal gradients under higher permeability and parabolic heating conditions.

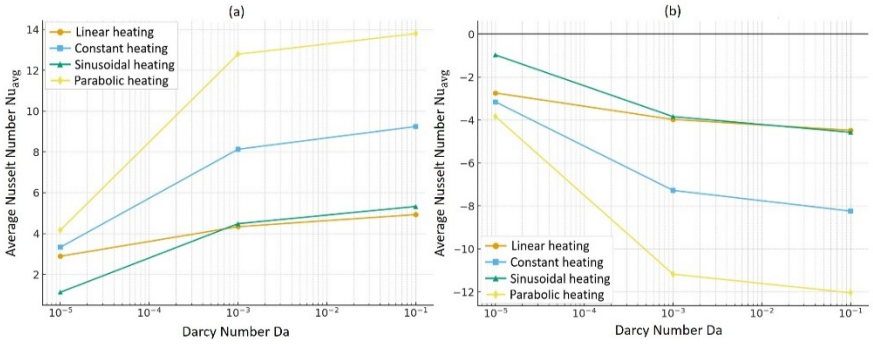

Figure 6 – Nu_{avg} distributions under different heating conditions along the bottom (a) and left (b) walls at Ra = 10^6

Entropy generation

This analysis examines the Bejan number for the four different heating conditions, with varying Rayleigh numbers ($Ra = 10^3\ and\ Ra = 10^6$), and Darcy numbers ($Da = 10^{-1}, 10^{-3}\ and\ 10^{-5}$).

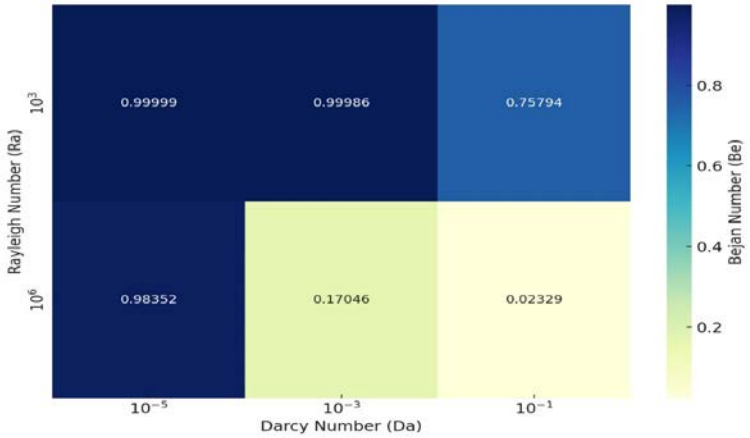

Figure 7 – Heat map of Be number depicting the influence of Ra and Da in case of constant heating from below

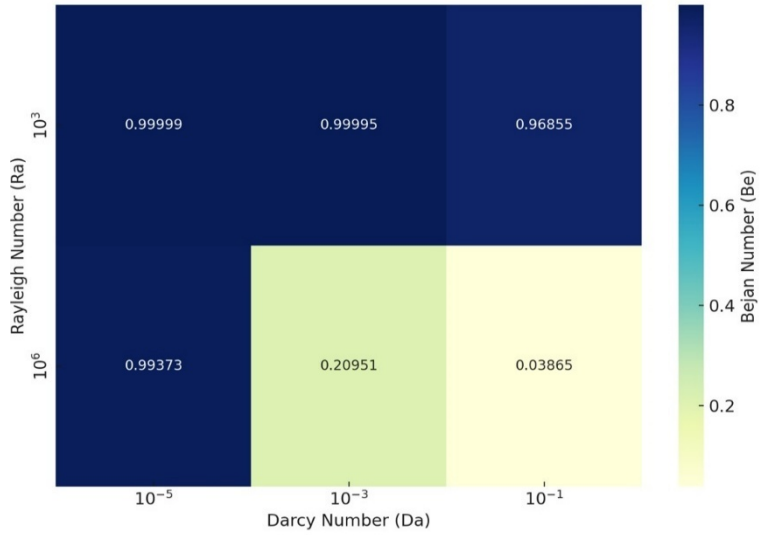

Figure 8 – Heat map of Be number depicting the influence of Ra and Da in case of linear heating from below

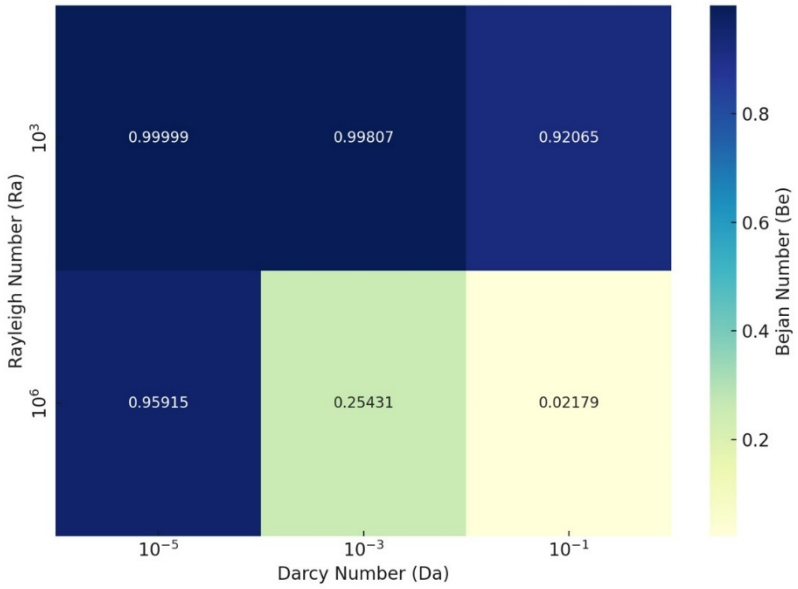

Figure 9 – Heat map of Be number depicting the influence of Ra and Da in case of quatratic heating from below

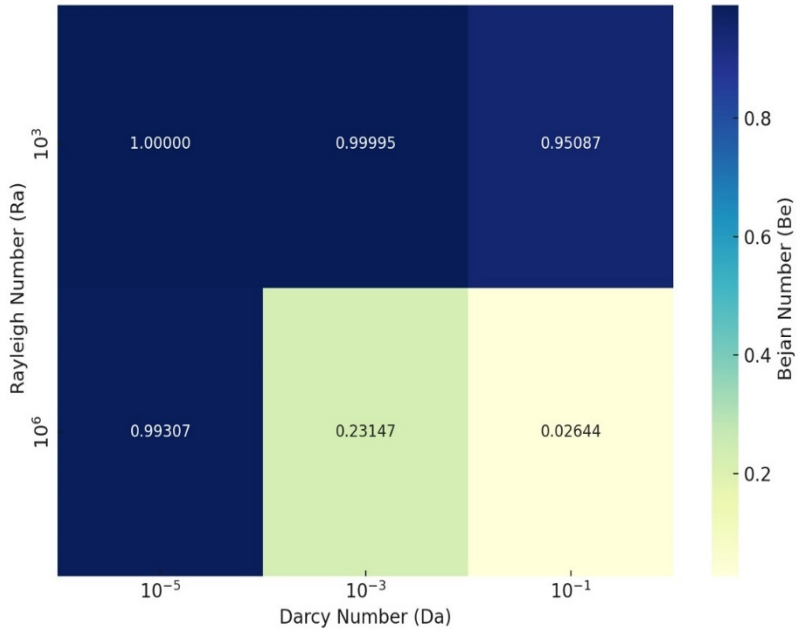

Figure 10 – Heat map of Be number depicting the influence of Ra and Da in case of sinusoidal heating from below

Across all four heating cases, thermal irreversibility dominates at low Rayleigh numbers $Ra = 10^3$, with the Bejan number remaining close to 1 for all Darcy numbers. This trend is consistent in linear, parabolic, sinusoidal, and constant heating cases, where fluid friction has a minimal effect. In contrast, for a Rayleigh number 10^6, the behavior shifts significantly. At high Rayleigh numbers and high permeability, fluid friction irreversibility dominates, particularly in the linear, parabolic, sinusoidal, and constant heating cases, with the Bejan number indicating strong convection effects. However, as the Darcy number decreases, the permeability decreases as well, and thermal irreversibility begins to take over. The Bejan number gradually increases towards 1, reflecting the increasing importance of thermal effects due to the suppression of convection and the rise in flow resistance. While the general trend of fluid friction dominance at higher Rayleigh numbers and lower permeability dominance at lower Rayleigh numbers holds true across all cases, the specific behavior of the Bejan number varies slightly based on the heating mode, with sinusoidal heating showing a more gradual transition compared to the others.

Practical applications

Although this study primarily focuses on numerical simulations, the insights gained have direct implications for real-world thermal systems. The influence of heating profiles and permeability on convective heat transfer is particularly relevant to cooling technologies such as electronic devices, heat exchangers, and energy storage systems, where efficient thermal management is crucial. Likewise, the balance between conduction and convection observed in porous cavities offers guidance for designing insulation materials in both construction and industry, especially under low-permeability conditions that minimize convective losses. In the biomedical field, porous media models are widely applied to tissue cooling, drug delivery, and cryopreservation; here, the demonstrated effects of sinusoidal and parabolic heating could support more effective localized thermal treatments and scaffold designs. Finally, the results also extend to renewable energy systems, including solar collectors and geothermal technologies, where the interplay between buoyancy-driven flow and porous structures governs overall thermal efficiency.

Table 2 – Nomenclature

Be	Bejan number
Be_{avg}	Average Bejan number
Da	Darcy number
g	Gravitational acceleration, ($m.s^{-2}$)
H	Height of the enclosure, (m)
k	Thermal conductivity, ($W.m^{-1}.\mathrm{K}^{-1}$)
K	Permeability, (m^2)
L	Length of the enclosure, (m)
Nu_L	Local Nusselt number
Nu_{avg}	Average Nusselt number
p	Pressure (Nm^{-2}))
P	Dimensionless pressure
Pr	Prandtl number
Ra	Rayleigh number
S	Dimensionless total entropy
S_T	Total entropy
S_{hti}	Dimensionless entropy generation due to heat transfer
S_{ffi}	Dimensionless entropy generation due to fluid friction
T	Temperature (K)
T_0	Bulk temperature $\frac{T_h+T_c}{2}$ (K)
u, v	Cartesian velocity components (m/s)

U, V	Dimensionless velocity components
X, Y	Dimensionless Cartesian coordinates
Greek symbols	
α	Thermal diffusivity, ($m^2 s^{-1}$)
β	Volumetric expansion coefficient, (K^{-1})
θ	Dimensionless temperature
μ	Dynamic viscosity, ($kg.m^{-1}.s^{-1}$)
λ	Wave amplitude
ν	Kinematic viscosity, ($m^2 s^{-1}$)
ε	Porosity
ξ	Irreversibility distribution ratio
ψ	Stream function
Subscripts	
avg	Average
c	Cold wall
h	Hot wall
max	Maximum
min	Minimum

Conclusion

This study comprehensively investigated the effects of heating methods and Darcy numbers ($Da = 10^{-5}, 10^{-3}$ and 10^{-1}) on fluid flow and heat transfer in a porous square cavity with sinusoidal vertical walls under a high Rayleigh number ($Ra = 10^6$). The results revealed that permeability and heating conditions significantly influence isotherm distribution, fluid circulation patterns and Nu_L variations. At low permeability $Da = 10^{-5}$, heat transfer is predominantly conductive, while at high permeability $Da = 10^{-1}$, convection becomes dominant. Different heating methods introduce distinct thermal and flow behaviors, but the overall trends remain consistent across the cavity. The key obtained findings are:

Increasing the Darcy number intensifies fluid circulation, with stronger vortices forming at higher permeability levels.

Linear, parabolic, sinusoidal, and constant heating profiles create distinct thermal gradients, influencing vortex strength and flow complexity.

Sinusoidal heating shows oscillatory trends in local Nusselt number, while permeability strongly affects heat flux distribution along the cavity walls.

At low Rayleigh numbers $Ra = 10^3$, thermal irreversibility dominates across all Darcy numbers. At high Rayleigh numbers $Ra = 10^6$, fluid friction irreversibility prevails at high Darcy numbers but shifts to thermal irreversibility as Darcy numbers decrease.

At low Rayleigh numbers $Ra = 10^3$, all heating methods show dominance of thermal irreversibility.

At high Rayleigh numbers $Ra = 10^6$, linear and parabolic heating exhibit stronger fluid friction irreversibility at higher Darcy numbers $Da = 10^{-1}$.

References

Böttcher, N., Watanebe, N., Görke, U. J., and Kolditz, O., 2016. Geoenergy Modeling I : Geothermal Processes in Factured Porous Media (Computational Modeling of Energy Systems). *Springer International Publishing*.

DOI:10.1007/978-3-319-31335-1

Abed Gatea Al-Shammary, A., Kouzani, A., Gyasi-Agyei, Y., Gates, W., and Rodrigo-Comino, J., 2020. Effects of solarisation on soil thermal-physical properties under different soil treatments: A review, *Geoderma,* 363, pp. 110038

https://doi.org/10.1016/j.geoderma.2019.114137

Kumar, D., Alam, M., Zou, P. X. W., Sanjayan, J. G., and Memon, R. A. 2020. Comparative analysis of building insulation material properties and performance, *Renewable and sustainable energy reviews,* 131, pp. 110038.

https://doi.org/10.1016/j.rser.2020.110038

Picher, C., Metzler, G., Niederegger, C., and Lacker, R. 2012. Thermo-mechanical optimization of porous building materials based on micromechanical concepts : Application to load-carring insulation materials.

https://doi.org/10.1016/j.compositesb.2011.09.013

Bloemendal, M., Olsthoom, T., and Boons, F., 2014. How to achieve optimal and sustainable use of the subsurface for Aquifer Thermal Energy Storage. *Energy Policy*, 66, pp 104-114

https://doi.org/10.1016/j.enpol.2013.11.034

Gao, D., Chen, Z., and Chen, L., 2014. A thermal lattice Bottzmann model for natural convection in porous media under local thermal non-equilibrium conditions. *International Journal of Heat and Mass Transfer*, 70, pp. 979-989.

https://doi.org/10.1016/j.ijheatmasstransfer.2013.11.050

Kaviany, M., 2011. Principles of heat transfer in porous media. *Mechanical Engineering Series*. Spring-Verlag New York Inc.

https://doi.org/10.1007/978-1-4612-4254-3

Basak, T., Kaluri, R.S. and Balakrishnan, A.R. 2011. Effects of Thermal Boundary Conditions on Entropy Generation during Natural Convection. *Numerical heat transfer. Part A. Applications.* 59(5), pp.372–402.

https://doi.org/10.1080/10407782.2011.549075

Kaluri, R.S. and Basak, T. 2011. Entropy generation due to natural convection in discretely heated porous square cavities. *Energy*, 36(8), pp. 5065–5080.
https://doi.org/10.1016/j.energy.2011.06.001
Brahmi, C.E., Maache, M., Belghar, N., Kalfali, M. and Bessaih, R. 2024. Free convection and entropy generation inside porous cavities with irregular vertical walls nonuniformly heated from below*. Numerical heat transfer. Part A. Applications.* pp.1–27.
https://doi.org/10.1080/10407782.2024.2359046
Dutta, S., Goswami, N., Pati, S. and Biswas, A.K. 2020. Natural convection heat transfer and entropy generation in a porous rhombic enclosure: influence of non-uniform heating. *Journal of Thermal Analysis and Calorimetry*, 144(4), pp.1493–1515.
https://doi.org/10.1007/s10973-020-09634-7
Tasmin, M., Nag, P., Hoque, Z.T. and Molla, Md. M. 2021. Non-Newtonian effect on heat transfer and entropy generation of natural convection nanofluid flow inside a vertical wavy porous cavity. *SN applied sciences*, 3(299).
https://doi.org/10.1007/s42452-021-04157-8
Al Waaly, A., Tumpa, S.A., Nag, P., Paul, A.R., Saha, G. and Saha, S.C. 2024. Entropy generation associated with natural convection within a triangular porous cavity containing equidistant cold domains. *Frontiers in Energy Research*, 12:1422256.
https://doi.org/10.3389/fenrg.2024.1422256
Rashad, A.M., Armaghani, T., Chamkha, A.J. and Mansour, M.A. 2018. Entropy generation and MHD natural convection of a nanofluid in an inclined square porous cavity: Effects of a heat sink and source size and location. *Chinese Journal of Physics*. 56(1), pp.193–211.
https://doi.org/10.1016/j.cjph.2017.11.026
Chen, X. B., Yu, P., Sui, Y., Winoto, S. H., and Low, H. T., 2008. Natural Convection in a Cavity Filled with Porous Layers on the Top and Bottom Walls. *Transport in Porous Media*.78(2), pp. 259-276.
https://doi.org/10.1007/s11242-008-9300-2
Bejan, A., 1979. A Study of Entropy Generation in Fundamental Convective Heat Transfer. *Journal of Heat Transfer*, 101(4) pp. 718-725.
https://doi.org/10.1115/1.3451063
Bhardwaj, S., Dalal, A., and Pati, S., 2015. Influence of wavy wall and non-uniform heating on natural convection heat transfer and entropy generation inside porous complex enclosure. *Energy.* 79 pp. 467-481.
https://doi.org/10.1016/j.energy.2014.11.036

Prirodna konvekcija i stvaranje entropije unutar porozne kvadratne šupljine sa neravnim vertikalnim zidovima u četiri režima zagrevanja

Mouna Maache, **autor za prepisku**, *Chihab* Eddine Brahmi, *Nourredine* Belghar, *Mahmoud* Kalfali
Faculty of Science and Technology, Department of Mechanical Engineering, Abbes Laghrour University, Khenchela, Algeria

OBLAST: mehanika, mašinstvo
TIP ČLANKA: originalni naučni rad

Sažetak:

Uvod/cilj: Ovaj rad proučava prirodnu konvekciju unutar porozne šupljine sa neravnim vertikalnim zidovima, sa težištem na ispitivanju uticaja različitih režima zagrevanja. Model se sastoji od kvadratne šupljine sa sinusoidnim neravninama na vertikalnim zidovima. Šupljina ima kvadratni poprečni presek, a neravnine su opisane sinusoidnom talasnom funkcijom sa određenom amplitudom i talasnom dužinom. Levi vertikalni zid šupljine održava se na konstantnoj niskoj temperaturi, dok je donji zid podvrgnut različitim profilima zagrevanja, uključujući linearno, konstantno, parabolično i sinusoidno zagrevanje. Izbor ovih različitih režima zagrevanja ima za cilj da ispita kako se ponašanje prenosa toplote menja u svakom režimu. Gornji i desni zid se smatraju adijabatskim.

Metode: Uticaj metoda zagrevanja i Darsijevog broja na strujanje fluida i prenos toplote pri visokom Rejnoldsovom broju analizira se numerički.

Rezultati: Rezultati pokazuju da svi profili zagrevanja stvaraju različite termičke gradijente koji utiču na jačinu vrtloga i složenost strujanja. U radu se ispituje i nepovratno ponašanje sistema sa fokusom na stvaranje entropije usled prenosa toplote i viskoznog trenja, a radi procene termodinamičke efikasnosti šupljine.

Zaključak: Cilj studije je da pruži sveobuhvatno razumevanje kako uslovi zagrevanja, promena permeabilnosti i konvekcija pri visokom Rejnoldsovom broju utiču na termičku i fluidnu dinamiku u poroznim šupljinama, kao i implikacije za unapređenje performansi sistema za upravljanje toplotom u praktičnim inženjerskim primenama.

Ključne reči: šupljina, porozna sredina, prirodna konvekcija, generisanje entropije, poroznost, permeabilnost.

Paper received on: 2 July 2025.
Manuscript corrections submitted on: 30 November 2025.
Paper accepted for publishing on: 22 January 2026.